Climatologies of nighttime upper thermospheric winds measured by ground-based Fabry-Perot interferometers during geomagnetically quiet conditions: 1. Local time, latitudinal, seasonal, and solar cycle dependence

J. T. Emmert,[1] M. L. Faivre,[2] G. Hernandez,[3] M. J. Jarvis,[4] J. W. Meriwether,[2] R. J. Niciejewski,[5] D. P. Sipler,[6] and C. A. Tepley[7]

Received 30 June 2006; revised 12 September 2006; accepted 21 September 2006; published 1 December 2006.

[1] We analyze ground-based Fabry-Perot interferometer observations of upper thermospheric (~250 km) horizontal neutral winds derived from Doppler shifts in the 630.0 nm (red line) nightglow. The winds were measured over the following locations: South Pole (90°S), Halley (76°S, 27°W), Arequipa (17°S, 72°W), Arecibo (18°N, 67°W), Millstone Hill (43°N, 72°W), Søndre Strømfjord (67°N, 51°W), and Thule (77°N, 68°W). We derive climatological quiet time ($Kp < 3$) wind patterns as a function of local time, solar cycle, day of year, and the interplanetary magnetic field (IMF), and provide parameterized representations of these patterns. At the high-latitude stations, and at Arequipa near the geomagnetic equator, wind speeds tend to increase with increasing solar extreme ultraviolet (EUV) irradiance. Over Millstone Hill and Arecibo, solar EUV has a negative effect on wind magnitudes. As represented by the 10.7 cm radio flux proxy, the solar EUV dependence of the winds at all latitudes is characterized by a saturation or weakening of the effect above moderate values ($F_{10.7} > 150$). The seasonal dependence of the winds is generally annual, but there are isolated cases in which a semiannual variation is observed. Within the austral winter, winds measured from the South Pole show a substantial intraseasonal variation only along longitudes directed toward the magnetic pole. IMF effects are described in a companion paper.

Citation: Emmert, J. T., M. L. Faivre, G. Hernandez, M. J. Jarvis, J. W. Meriwether, R. J. Niciejewski, D. P. Sipler, and C. A. Tepley (2006), Climatologies of nighttime upper thermospheric winds measured by ground-based Fabry-Perot interferometers during geomagnetically quiet conditions: 1. Local time, latitudinal, seasonal, and solar cycle dependence, *J. Geophys. Res.*, *111*, A12302, doi:10.1029/2006JA011948.

1. Introduction

[2] Neutral winds are a key component of the coupled thermosphere-ionosphere system. Thermospheric neutral winds play a direct role in the transport of ionospheric plasma along magnetic field lines and in the generation of electric fields via wind dynamos. Indirectly, winds can alter the ionospheric composition via changes in the neutral composition. They also modulate ionospheric phenomena such as equatorial spread *F*, scintillation, and high-latitude convection. In this paper we analyze climatological winds during geomagnetically quiet conditions; wind patterns can change dramatically during geomagnetic storms [e.g., *Hernandez et al.*, 1980; *Wickwar et al.*, 1984; *Emmert et al.*, 2002; *Richmond et al.*, 2003].

[3] Drawing on long-term ground-based measurements, numerous studies have examined the climatology of quiet time upper thermospheric (above ~200 km) neutral winds, including the effects of local time, season, and solar cycle phase [e.g., *Hernandez and Roble*, 1984; *Biondi et al.*, 1990, 1999; *Hedin et al.*, 1991; *Duboin and Lafeuille*, 1992; *Crickmore*, 1994; *Killeen et al.*, 1995; *Aruliah et al.*, 1996; *Miller et al.*, 1997; *Buonsanto and Witasse*, 1999; *Igi et al.*, 1999; *Kawamura et al.*, 2000; *Griffin et al.*, 2004]. The coupled seasonal and solar cycle dependence of nighttime quiet time winds has been examined in less detail, but a few interesting features have been observed. *Emmert et al.* [2003] showed that the meridional winds north of Millstone Hill exhibit a semiannual variation during very low solar activity conditions and an annual variation at other times. *Aruliah et al.* [1996] reported that an equinoctial asymmetry

[1] E. O. Hulburt Center for Space Research, U.S. Naval Research Laboratory, Washington, D.C., USA.
[2] Department of Physics and Astronomy, Clemson University, Clemson, South Carolina, USA.
[3] Department of Earth and Space Sciences, University of Washington, Seattle, Washington, USA.
[4] British Antarctic Survey, Cambridge, UK.
[5] Space Physics Research Laboratory, University of Michigan, Ann Arbor, Michigan, USA.
[6] Haystack Observatory, Massachusetts Institute of Technology, Westford, Massachusetts, USA.
[7] Arecibo Observatory, Cornell University, Arecibo, Puerto Rico.

Copyright 2006 by the American Geophysical Union.
0148-0227/06/2006JA011948

Table 1. Data Sets Used in This Study

Station	Geographic Latitude	Magnetic (QD) Latitude	Geographic Longitude	Years of Data	Number of Nights	Seasonal Coverage
Thule	76.5°N	84.6°N	68.4°W	1987–1989	145	Sep–Mar
Søndre Strømfjord	67.0°N	73.3°N	51.0°W	1983–1984, 1987–1994, 2002–2004	940	Sep–Apr
Millstone Hill	42.6°N	53.1°N	71.5°W	1989–2002	1177	All
Arecibo	18.4°N	29.1°N	66.8°W	1980–1999	368	All
Arequipa	16.5°S	3.5°S	71.5°W	1983–1990, 1997–2001	922	Feb–Nov
Halley	75.5°S	61.6°S	26.6°W	1988–1998	572	Mar–Sep
South Pole	90.0°S	74.2°S	N/A	1989–1999	968	Apr–Sep

observed in high-latitude meridional winds is more pronounced during solar maximum, and at low latitudes, the results of *Biondi et al.* [1991, 1999] suggest interactive influences of season and solar flux on the winds.

[4] Most of the studies cited above utilized data taken prior to 1991. Over the past 10–15 years, ground-based Fabry-Perot spectrometer (usually termed Fabry-Perot interferometers, or FPIs) measurements of nighttime upper thermospheric winds have further accumulated to a degree that permits seasonal and solar cycle effects to be examined in unprecedented detail at a number of stations from the South Pole to the northern polar cap. In this paper, we analyze the local time, day-of-year, and solar cycle climatology of quiet time nighttime winds over seven stations. In addition to studying quiet time wind climatology in its own right, one objective of this study is to establish quiet time baselines for use in analyzing storm-induced wind perturbations. Therefore we also develop empirical parametric representations of the data and provide in the auxiliary material[1] the coefficients and other information needed to evaluate these models. The models for the midlatitude and high-latitude stations also represent the effect of the dawn-dusk component of the interplanetary magnetic field (IMF B_y), which strongly influences high-latitude neutral wind patterns [e.g., *Meriwether and Shih*, 1987], and the model for one polar cap station includes quiet time effects of the IMF north-south component (IMF B_z). The IMF dependences are discussed in a companion paper [*Emmert et al.*, 2006, hereinafter referred to as Paper 2].

2. Data

[5] We analyze ground-based FPI observations of upper thermospheric horizontal winds derived from Doppler shifts in the 630.0 nm (red line) nightglow. The height of the peak emission is generally near 250 km but varies with solar zenith angle and solar cycle. We analyze data from a variety of stations covering all latitudes; these data are contained in the CEDAR database (http://cedarweb.hao.ucar.edu). Only data from geomagnetically quiet conditions, defined as 3-hour $Kp < 3$, were used. A more restrictive criterion (e.g., by placing limits on the previous indices as well) might further reduce the effects of geomagnetic activity on the results. However, since the timescale of the wind response to geomagnetic disturbances varies with latitude, we opted for a simple (and somewhat arbitrary) statistical criterion that can be uniformly applied to data from all latitudes. In addition, this straightforward selection of quiet time conditions facilitates the analysis and statistical interpretation of perturbation winds computed from the quiet time baseline.

[6] For stations that monitor cloud cover conditions and take measurements in all weather, we restricted our analysis to periods for which the cloud cover index (a scale of 0–10) is less than or equal to 3.

[7] Table 1 summarizes the location and statistical coverage of each quiet time data set, including the number of nights meeting the quiet time and cloud cover criteria. The coordinates are given for the observing site, but the location of the measured airglow depends on the effective height of the emission and the elevation angle of the instrument; for typical values of 250 km and 30°, respectively, the measured wind is about 4° of latitude away from the station. Note that for the South Pole, this means that the latitude of all the measurements is ~86°S. The magnetic latitudes given in the table are the quasi-dipole (QD) latitudes described by *Richmond* [1995].

[8] Detailed descriptions of each instrument can be found in the informational files that accompany each data set on the CEDAR database and in the references cited below. In the following sections, we briefly describe the observing modes of each instrument and the geometrical characteristics of the measurements.

2.1. Thule

[9] This limited data set covers low solar activity conditions during October–November of 1987 and moderate-to-high solar activity during the winter of 1988–1989. The observations were made in the cardinal directions at an elevation of 45°; the data are evenly divided among the four directions. The zero-wind reference was obtained for each night by averaging Doppler shifts measured in the zenith direction. Detailed descriptions of the instrument may be found in the work of *Meriwether et al.* [1983, 1988] and *Killeen et al.* [1983, 1995]. The most recent climatological analysis of these data was presented by *Killeen et al.* [1995].

2.2. Søndre Strømfjord

[10] In the routine observing mode, measurements were made in the cardinal directions at an elevation of 45°, and these are the only observations used in this study. The zero-wind reference was obtained for each night by averaging Doppler shifts measured in the zenith direction. Details of the instrument and operation may be found in the work of *Meriwether et al.* [1983, 1988], *Killeen et al.* [1983, 1995],

[1] Auxiliary materials are available in the HTML. doi:10.1029/2006JA011948.

and *Niciejewski et al.* [1989]. The most recent climatological analysis, using 1985–1991 data, was presented by *Killeen et al.* [1995].

2.3. Millstone Hill

[11] In the standard operating mode, four measurements were made at an elevation of 30° and at azimuths of (315°, 45°) and (135°, 225°), along with a fifth measurement in the zenith direction. In this mode, the line-of-sight wind measurements were used to derive the horizontal vector winds to the north and south of the observatory, assuming negligible longitudinal gradients and vertical winds. We used these data as well as a few (∼10%) meridional wind measurements made at azimuths of 0° and 180° and at various elevations. The zero wind reference used to calibrate the measurements was obtained by smoothing and interpolating each night's series of zenith observations. The instrument and its operation were described by *Sipler et al.* [1991] and *Buonsanto et al.* [1992]. *Fejer et al.* [2002] and *Emmert et al.* [2003] conducted the most recent climatological analyses, using 1991–2001 data.

2.4. Arecibo

[12] Measurements were made in eight evenly spaced azimuthal directions, at an elevation of 30°. Each azimuthal scan was used to derive, via a second order Taylor expansion, overhead vector winds. For about half of the derived wind data, zenith observations were used as a zero wind reference; for the other half, nightly averages of the derived vertical winds were used. Detailed information about the instrument may be found in the work of *Burnside et al.* [1981] and *Burnside and Tepley* [1989]. The most recent climatological analysis was performed by *Biondi et al.* [1999], using 1980–1990 data.

2.5. Arequipa

[13] The 1983–1990 measurements were made in the four cardinal directions at an elevation of 30°, along with a fifth measurement in the zenith direction. The zero wind reference used to calibrate the measurements was obtained by smoothing and interpolating each night's series of zenith observations. The 1983–1990 data used in this study are the same data analyzed by *Biondi et al.* [1999], except that we excluded observations made between dusk and 2100 LT; during this time period the 1983–1990 measurements are anomalously more northward and eastward than the newer, more accurate 1997–2001 measurements. Otherwise, the data from the two time periods are in very good climatological agreement.

[14] The 1997–2001 measurements were made at an elevation of 30° in four azimuthal directions: 350°, 80°, 170°, and 260° (N, E, S, and W; the 10° offset facilitates bistatic measurements with an FPI in Chile). The N, E and S, W pairs in this slightly rotated coordinate system were each transformed to obtain two (N and S) geographic meridional and two (E and W) geographic zonal wind observations. A zero-wind reference was obtained for each night by averaging Doppler shifts measured in the zenith direction.

[15] Detailed information about the instrument may be found in the work of *Biondi and Sipler* [1985], *Meriwether et al.* [1997], and *Faivre et al.* [2006]. The most recent climatological wind analysis was performed by *Biondi et al.* [1999], using the 1983–1990 data.

2.6. Halley

[16] Measurements were made in the four cardinal directions at an elevation of 30° and in the zenith direction. A zero-wind reference was obtained for each night by averaging Doppler shifts measured in the zenith direction. The derived horizontal wind measurements in each direction were fit to cubic splines in universal time; in the data records, fitted values are reported every 15 min. The 1994–1998 data records combine and average north/south and east/west data to produce an estimate of the overhead wind vector; in these records, values are given at 30 min intervals. In our analyses of these data, we gave the 1994–1998 data four times more weight relative to the 1988–1993 data, in order to accommodate the lower sampling rate (one record every 30 min versus two records every 15 min) of the later data records. Details of the instrument are given by *Stewart et al.* [1985] and *Stewart* [1986]. To date, the only climatological analysis of Halley winds was conducted by *Crickmore* [1994], using data from 1988–1992.

2.7. South Pole

[17] Measurements were made in eight evenly spaced azimuthal directions at an elevation of 30°. A zero-wind reference was obtained by computing long-term (months) averages of zenith observations. Each of the eight line-of-sight measurements is used to produce the northward component of the horizontal wind at a different longitude (30°E, 75°E, etc.). Assuming a red line emission height of 250 km, the effective geographic latitude of the observations is ∼86°S. After obtaining empirical models for each look direction, we partially combined them to obtain a vector wind field, as described in section 3.3.

[18] Details of the South Pole FPI and its operation may be found in the work of *Hernandez and Mills* [1973] and *Hernandez et al.* [1990]. The analysis of 1989 data by *Hernandez et al.* [1991] is the only previously available climatology of South Pole FPI winds.

3. Analysis and Empirical Model Development

3.1. Parameters Considered

[19] We analyze the data as a function of local solar time, solar EUV irradiance, day of year, and IMF B_y and B_z (in geocentric solar magnetospheric, or GSM, coordinates). Local solar time is defined here as the local apparent time at the measurement location (as opposed to the local mean time at the instrument site). The solar 10.7 cm radio flux ($F_{10.7}$), which is measured daily at 2000 UT from Penticton, Canada (1700 UT from Ottawa prior to 1991) is used as a proxy for EUV irradiance conditions. The integer day-of-year (day 1 = 1 Jan 0000–2359 UT) is used to represent the seasonal behavior of the data.

[20] At high latitudes, winds are known to have a strong dependence on the interplanetary magnetic field [e.g., *Meriwether et al.*, 1973; *Rishbeth*, 1977; *McCormac and Smith*, 1984; *Hernandez et al.*, 1991; *Richmond et al.*, 2003]. Under the quiet conditions we consider in this paper, the influence of B_z is generally weak (partly owing to the anticorrelation, about −0.36, between *Kp* and B_z), and the

Table 2. Parameterization of Empirical Models

Station	Local Time, LST	Day of Year, DAY	F10.7	IMF By	Coupled Terms (Full Coupling of Indicated Parameter Bases, Unless Noted)
Thule	Per. cubic splines	None	Piecewise linear	Linear (Also Bz)	LST × F10.7 LST × By: (including with a linear F10.7 term) LST × Bz
Søndre Strømfjord	Per. cubic splines	Annual terms	Piecewise linear	Linear	LST × DAY (nightside only) LST × F10.7 (nightside only) LST × By: (nightside only, including with a linear F10.7 term)
Millstone Hill	Per. cubic splines	Annual and semiannual terms	Piecewise linear	Linear	LST × DAY (nightside only) LST × F10.7 (nightside only) LST × By: (nightside only, including with a linear F10.7 term) LST × DAY × F10.7 (nightside only) LST × DAY × By (nightside, annual only)
Arecibo	Per. cubic splines	Annual and semiannual terms	Piecewise linear	None	LST × DAY (nightside, annual only) LST × F10.7 (nightside only) LST × DAY × F10.7 (midnight, semi-annual, high-F10.7 only)
Arequipa	Per. cubic splines	Annual terms	Piecewise linear	None	LST × DAY (nightside only) LST × F10.7 (nightside only)
Halley	Per. cubic splines	Annual terms	Piecewise linear	Linear	LST × DAY (nightside only) LST × F10.7 (nightside only) LST × By: (nightside only, including with a linear F10.7 term)
South Pole	Per. cubic splines (2.4-hour spacing)	Annual terms	Piecewise linear (w/extra node at 110)	Linear	LST × DAY LST × F10.7 LST × By (including with a linear F10.7 term)

winds are most responsive to B_y. However, at the magnetic polar cap station of Thule, quiet time B_z effects are significant. We use a ground-based proxy [*Vennerstroem et al.*, 2001; *Richmond et al.*, 2003] to represent IMF conditions; this proxy and the IMF dependence of the high-latitude winds are presented in Paper 2. In this paper, we focus on the local time, solar EUV, and day-of-year dependence of the winds.

[21] We analyze the data by sorting them into multiparameter bins and computing the average and estimated uncertainty of the mean for each bin. Outliers greater than 3 s.d. away from the raw mean are discarded. The estimated error of the mean (e.e.m.) is computed by dividing the sample standard deviation by the square root of the number of nights in the sample [e.g., *Emmert et al.*, 2002]. This method produces a larger and more realistic estimate of the uncertainty in the computed mean than the usual method of dividing by the square root of the sample size, since thermospheric measurements are typically highly correlated on timescales less than 1 day. In assessing whether the localized effect of a given parameter (or combination of parameters) is statistically significant, we consider the following criteria: (1) Is the difference in the average winds from two parameter bins larger than the corresponding uncertainties of the mean (i.e., no overlap of the 1 e.e.m. error bars)? (2) Does the effect show a consistent progression from one bin to the next (e.g., do the winds get progressively larger with increasing $F_{10.7}$)? (3) Is the effect consistent across bins of another parameter (e.g., is an $F_{10.7}$ trend seen during multiple seasons or in different local time sectors)? The application of these criteria is somewhat subjective, but in general we consider a feature that meets two out of three to be significant.

3.2. Empirical Models

[22] In order to further smooth the data, and to provide a tool for specifying climatological winds and a quiet time baseline, we developed parametric representations of the data. The basis functions for each model parameter and the degree of coupling among the parameters were chosen in an effort to represent the climatological features deemed significant, without overfitting the data. We also endeavored to minimize the number of terms in each model; however, if terms were necessary for one wind component then we also used them for the other component even if they did not improve the fit. The models constitute a compact representation of the mean quiet time behavior of these extensive data sets.

[23] For the local time dependence, we used a basis of six periodic cubic B splines [e.g., *DeBoor*, 1978] with nodes at {0100, 0330, 0600, 1800, 2030, 2300} LT; these are the same functions used by *Emmert et al.* [2003] to represent the local time dependence of Millstone Hill FPI winds. The concentration of nodes in the nighttime sector and the absence of nodes during the day allows the model to flexibly represent the local time dependence where data exists without becoming unstable where there is no data. Also, the use of spline functions permits localized coupling with other parameters. We generally only coupled the $F_{10.7}$ and seasonal dependence with the four splines centered on midnight; this strategy greatly stabilized the behavior of the models near the dawn and dusk fringes of the data. In the case of the South Pole data, the local time coverage is continuous, and we used a basis of 10 periodic cubic splines with evenly spaced nodes.

[24] For the seasonal dependence, we used harmonic terms in day-of-year. In most cases, only terms representing annual variations were employed, but in some cases semiannual terms were also used. Most of the data sets do not

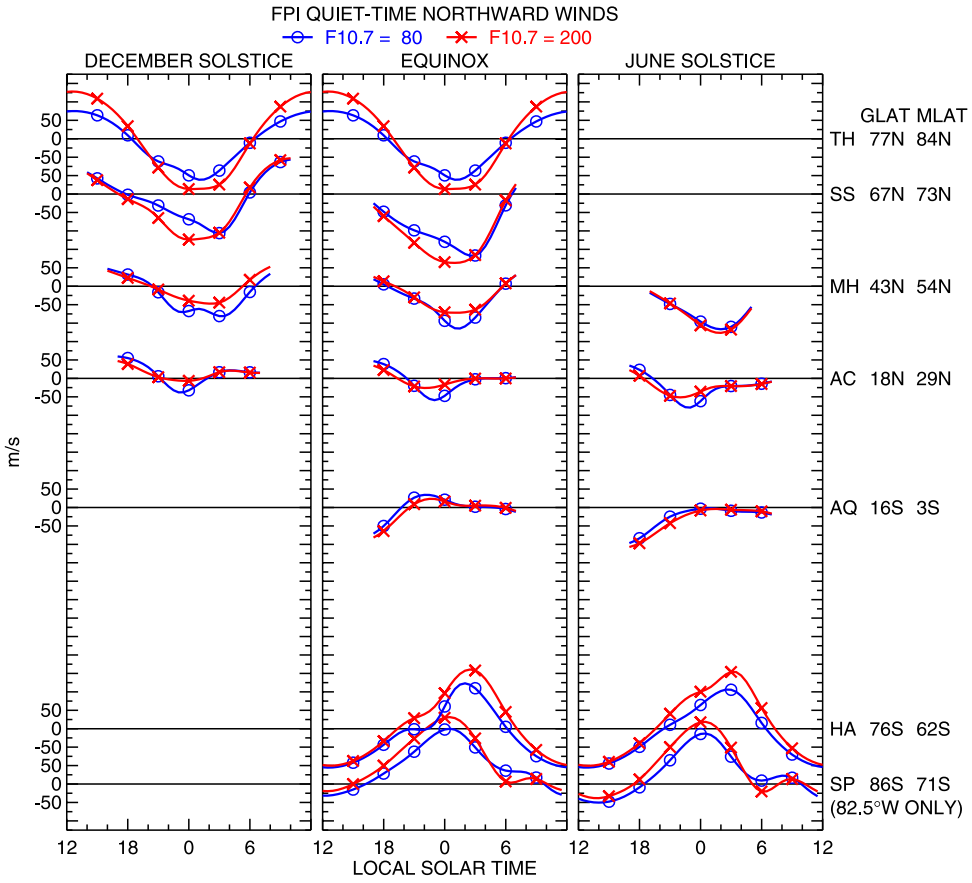

Figure 1. Meridional winds from the quiet time empirical models as a function of local solar time, for low ($F_{10.7}$ = 80, blue circles) and high ($F_{10.7}$ = 200, red crosses) solar EUV flux conditions. Results are stacked according to the geographic latitude of each station, and the separation between each reference axis roughly corresponds to the latitude separation between stations. The geographic and magnetic latitudes of the stations are given on the right; TH stands for Thule, SS stands for Søndre Strømfjord, MH stands for Millstone Hill, AC stands for Arecibo, AQ stands for Arequipa, HA stands for Halley, and SP stands for South Pole. Results are shown for day-of-year 0 (left), 90 (center), and 180 (right). The Millstone Hill results are for the north-looking direction. The South Pole results are for the 82.5°W longitude sector and were inferred from the 60°W and 105°W meridional wind models, as described in section 3.3. Note that the Thule model does not vary with season, so the same wind pattern is shown in the December solstice and equinox columns.

have year-round coverage, and in these cases the day-of-year expansion only represents intra-seasonal variations.

[25] The $F_{10.7}$ dependence is represented by piecewise linear functions, with a node at 140 (Arequipa model) or 160 (all other models); the South Pole model includes an additional node at 110. This scheme was chosen to represent the saturation of the $F_{10.7}$ effect at moderate to high levels of EUV irradiance (section 4.2). We implemented the piecewise linear representation using a basis of linear B splines; this is a convenient approach because the continuity constraints are implicitly imposed by the spline functions.

[26] Finally, the IMF B_y dependence and the B_z dependence (at Thule only) were represented by linear terms. These parameters were not used in the case of the low-latitude Arequipa and Arecibo data sets, where we did not detect any IMF effects. The effect of IMF on the midlatitude and high-latitude winds is discussed in Paper 2; the results shown in this paper represent B_y = 0 nT and, for Thule, B_z = 1 nT conditions.

[27] Table 2 summarizes the parameterization of each model, including the coupling among the various parameters. A full listing of the terms for each model is given in the auxiliary material.

[28] We generated models independently for each wind component (zonal and meridional). Except for the Millstone Hill and South Pole data, we combined data from different azimuthal directions (north + south and east + west). For the Millstone Hill data, we processed the north-looking and south-looking data (each consisting of both meridional and zonal winds) separately, due to the strong latitudinal gradients observed in the data [*Emmert et al.*, 2003]. For the South Pole models, we generated a meridional wind model for each of the eight azimuthal directions (corresponding to eight geographic longitudes), since the winds vary widely with direction. From these eight models, we also inferred vector wind fields as described in section 3.3.

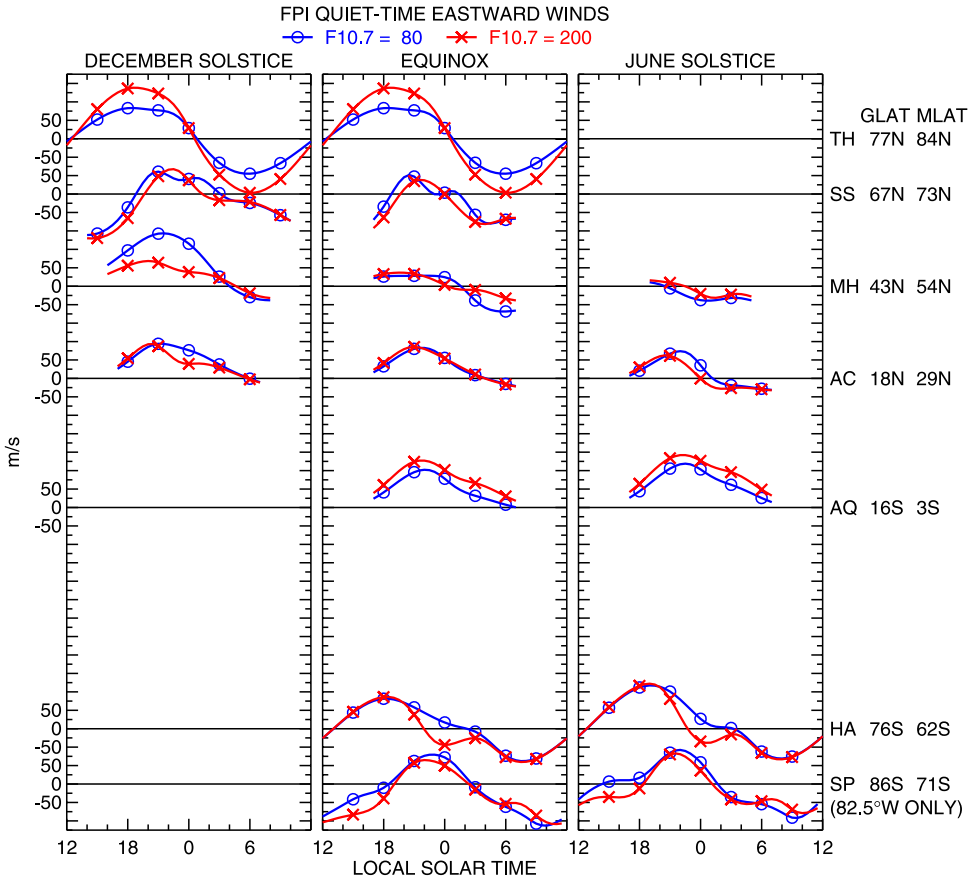

Figure 2. Same as Figure 1, except that the zonal component is shown. The South Pole zonal winds were inferred from the 60°W and 105°W meridional wind models, as described in section 3.3.

[29] The models are linear with respect to the coefficients, and we computed the coefficients for each model using a straightforward least-squares inversion. Outliers greater than 3 standard deviations (the root-mean-square residual) away from the initial fit were discarded, and a revised fit was computed. The model terms and coefficients are given in the auxiliary material, along with a table showing the mean and standard deviations of model residuals (data minus corresponding model values) for different $F_{10.7}$ conditions. The mean residuals are close to zero, which implies that the data are unbiased relative to the models; this is an expected consequence of the least-squares fitting process. Typical deviations of the measurements from the models are 35–85 m/s, depending on the station, wind component, and solar activity. Also provided in the auxiliary material are plots of the spline bases, along with Interactive Data Language (IDL) code for generating B splines. Code for evaluating the models is available from the CEDAR database at http://cedarweb.hao.ucar.edu/tools/empirical_models.html.

3.3. Derivation of Vector Wind Fields From the South Pole Empirical Models

[30] To derive the quiet time climatological wind field over the South Pole, we first evaluated all eight meridional wind models at a specified UT. Then, we combined neighboring (separated by 45° of longitude) meridional wind values to obtain vector winds at the midpoint, assuming a constant wind field between the two endpoints. This approach is similar to that used to derive vector winds from the Millstone Hill line-of-sight winds (section 2.3), except that the azimuthal spacing here is 22.5°, and we use the average line-of-sight (meridional) winds from the empirical model, rather than the raw measurements. We repeated this calculation for all eight neighboring pairs of longitudes to obtain vector winds at 7.5°E, 52.5°E, etc. Note that although the zonal component is not defined at the pole, the wind measurements were made ~4° north of the South Pole (section 2.7), where there is no ambiguity. The uncertainty of the mean meridional winds represented by the empirical models is on the order of 10 m/s (based on the e.e.m. of the binned averages and the scatter of the binned averages around the model); in the combined winds, this uncertainty is amplified by a factor of 1/cos(22.5°) = 1.08 for the meridional component and 1/sin(22.5°) = 2.61 for the zonal component.

4. Results and Discussion

4.1. Local Time Dependence

[31] Figures 1 and 2 show the meridional and zonal model results as a function of local solar time. At all stations, the meridional winds are predominately equatorward in the nighttime (1800–0600) sector. In the case of the South Pole FPI, only the results from 82.5°W (roughly the same meridian as the other stations) are shown; the meridional and zonal components were inferred from the 60°W and 105°W meridional wind models, as described in section

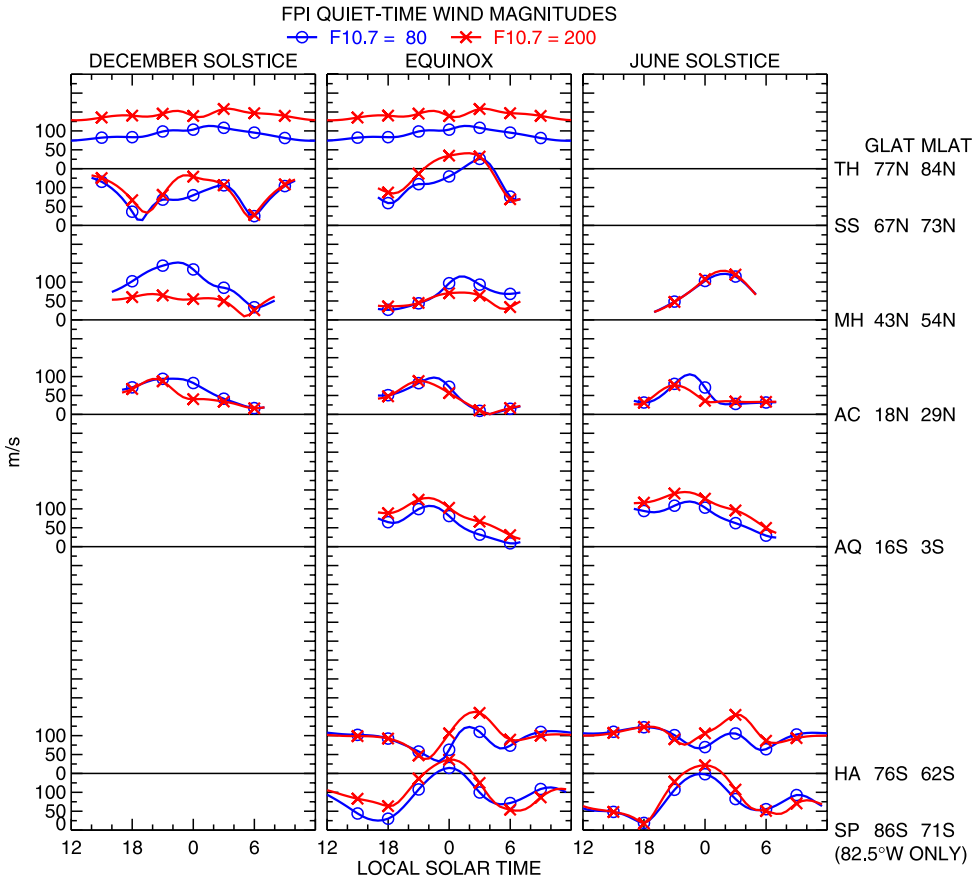

Figure 3. Same as Figure 1, except that the magnitude of the model horizontal wind vector is shown.

3.3. Peak equatorward wind magnitudes range from less than 50 m/s at low latitudes to 150–200 m/s at high latitudes. The peak generally occurs around 2200 at low latitudes and between 0000 and 0300 LT at middle and high latitudes.

[32] The zonal winds at middle and low latitudes (Millstone Hill, Arecibo, and Arequipa) are mainly eastward throughout the night, with peak magnitudes up to 150 m/s. At high latitudes, the zonal circulation is less uniform owing to the influence of ionospheric convection; the local time dependence of these winds is described in more detail in Paper 2.

4.2. Solar EUV Dependence

[33] The local time dependence of the midlatitude and low-latitude winds largely reflects the global circulation set up by pressure gradients induced by EUV heating [e.g., *Dickinson et al.*, 1984]; solar EUV might therefore expected to have a strong influence on wind magnitudes. The increased forcing associated with increased EUV irradiance is generally opposed by a corresponding increase in ion densities and hence ion drag [e.g., *Kawamura et al.*, 2000; *Fesen et al.*, 1986]. Figures 1 and 2 indicate that at Millstone Hill and Arecibo, the wind magnitudes tend to be smaller at solar maximum, in agreement with most previous midlatitude and low-latitude climatologies [e.g., *Buonsanto and Witasse*, 1999; *Biondi et al.*, 1999; *Fejer et al.*, 2002]. At the other stations, the increased EUV is generally associated with stronger winds. This is shown more directly in Figure 3, which depicts wind speeds derived from Figures 1 and 2. The difference between wind magnitudes associated with $F_{10.7} = 80$ (near solar minimum) and $F_{10.7} = 200$ (near solar maximum) is generally 25–50 m/s; the largest effect (~150 m/s) is seen during the winter solstice at Millstone Hill.

[34] At the latitudes of Millstone Hill and Arecibo, the increased ion drag at solar maximum apparently wins out over the increased pressure gradients, reducing the wind speeds. At Millstone Hill, however, some of the $F_{10.7}$ dependence could be due to changes in the relative importance of high-latitude heating and momentum sources, as suggested by *Hagan* [1993]. It is not obvious why a positive effect is observed at Arequipa, but perhaps the prereversal enhancement of F region vertical plasma drifts, which increases with increasing $F_{10.7}$ [*Fejer et al.*, 1991], plays a role in modulating zonal wind speeds along the magnetic equator. This kind of interpretation is difficult to establish unambiguously [*Biondi et al.*, 1999], however, because the effective height of the wind measurements also changes with the changing plasma profile [e.g., *Link and Cogger*, 1988].

[35] At high latitudes, ion drag is a major momentum source (rather than an impediment) for the neutrals [*Meriwether et al.*, 1973; *Roble et al.*, 1982], so increased ion densities (relative to the neutral density) associated with solar maximum perhaps explain the larger wind magnitudes under these conditions. The transition from a negative effect to a positive effect occurs between the latitudes of Millstone

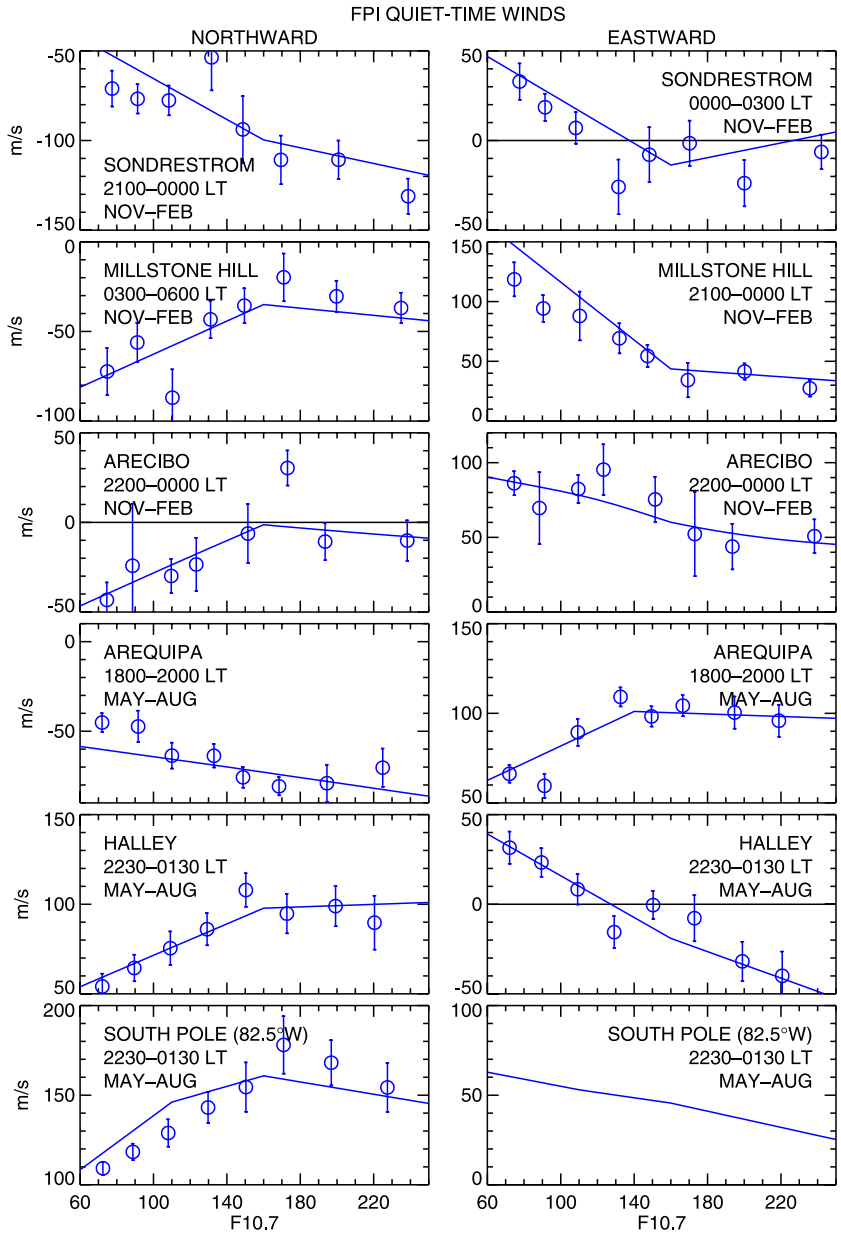

Figure 4. Average quiet time meridional (left column) and zonal (right column) winds as a function of $F_{10.7}$, in selected local time sectors during winter solstice (November–February in the northern hemisphere, May–August in the southern hemisphere). The data were sorted and averaged in the following $F_{10.7}$ bins: 60–80, 80–100, 100–120, 120–140, 140–160, 160–180, 180–220, and 200–400. The error bars denote the estimated uncertainty of the mean. The solid lines show corresponding results from the empirical models. The selected local time sectors generally correspond to the time of the strongest $F_{10.7}$ dependence. The Millstone Hill results are for the north-looking direction. The South Pole results are for the 82.5°W longitude sector; in this case, the raw meridional wind data from 60°W and 105°W were combined to produce the binned averages, and the model results are the vector winds derived from the meridional wind empirical models at the same two longitudes, as described in section 3.3.

Hill (54° magnetic) and Halley (62° magnetic). As at low latitudes, interpretation of solar cycle effects is complicated by the changes in the height of the emission layer.

[36] A common feature of the $F_{10.7}$ dependence of the winds from all stations is a saturation of the effect at moderate to high values, as shown in Figure 4, which depicts binned averages of data from selected winter local time sectors as a function of $F_{10.7}$, along with corresponding results from the empirical models. The South Pole meridional and zonal components were inferred from the 60°W and 105°W meridional wind models, as described in section 3.3; the meridional wind binned averages include 60°W and

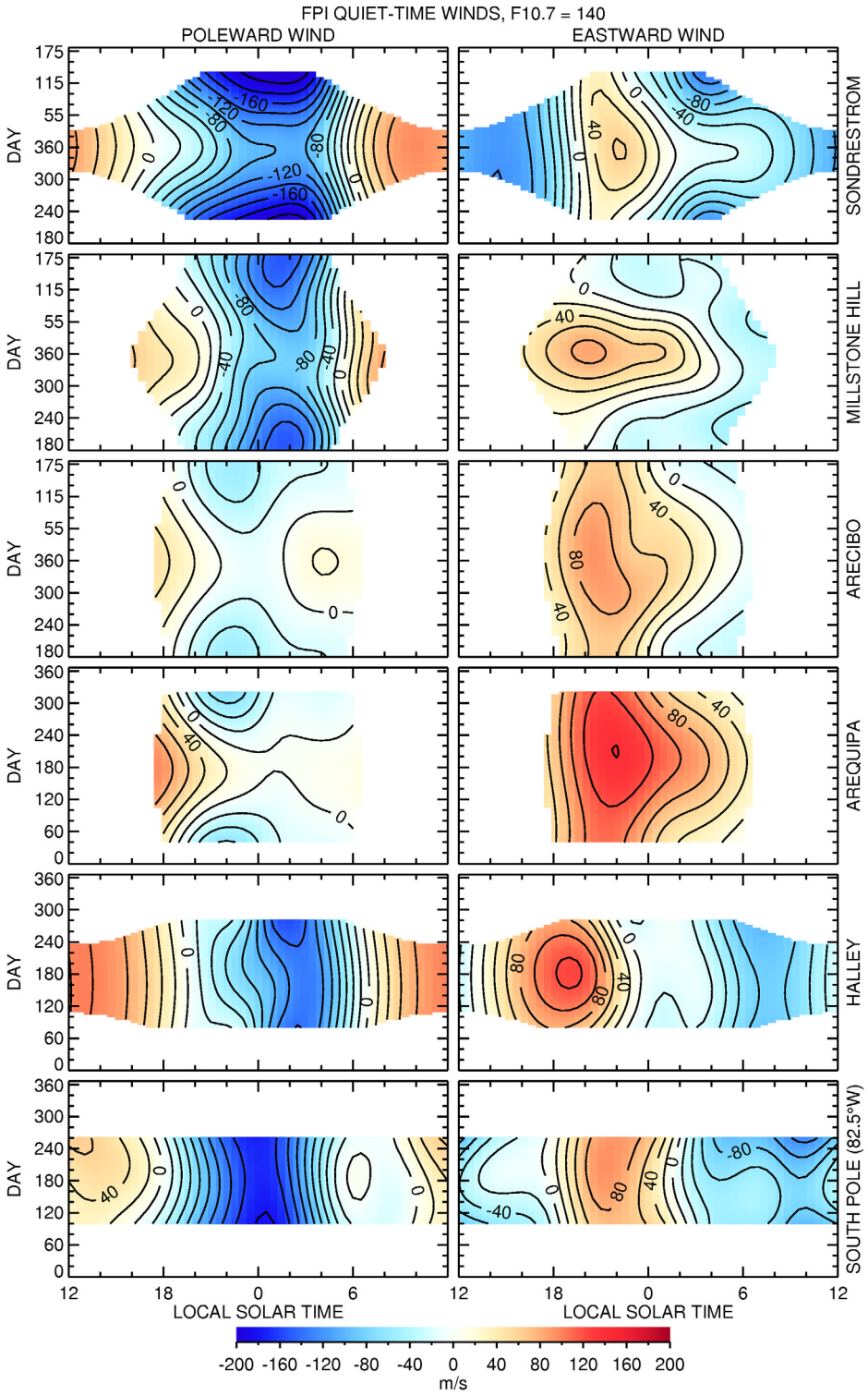

Figure 5. Quiet time (left) meridional and (right) zonal winds from the empirical models as a function of local time and day of year, for moderate ($F_{10.7}$ = 140) solar EUV conditions. For the meridional component, positive values (red) correspond to poleward winds. Note the different day-of-year axes for the northern and southern hemisphere stations; in all cases, the plotted results are centered on the winter solstice. The Millstone Hill results are for the north-looking direction. The South Pole results were inferred from the 60°W and 105°W meridional wind models, as described in section 3.3. The contour interval is 20 m/s.

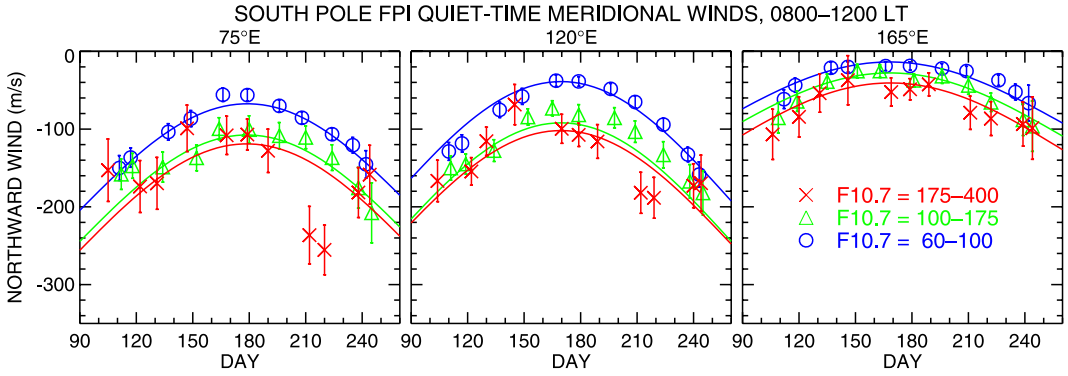

Figure 6. Average quiet time South Pole meridional winds as a function of day of year, in the 0800–1200 LT sector and along three longitudinal directions (left: 75°E, center: 120°E, right: 165°E). Results are shown for three solar EUV irradiance conditions: low (blue circles, $F_{10.7} < 100$), moderate (green triangles, $100 < F_{10.7} < 175$), and high (red crosses, $F_{10.7} > 175$). The day-of-year bins used to sort the data are 30 days wide and spaced at 15-day intervals. Error bars denote the estimated uncertainty of the mean. The smooth curves show corresponding results from the empirical models.

105°W data. At each station, the local time bins were chosen to highlight the strongest $F_{10.7}$ effects, but the results are typical of other conditions. The results indicate that the slope of the $F_{10.7}$ effect changes between $F_{10.7} = 140$ and $F_{10.7} = 160$, either leveling off completely or simply diminishing in magnitude.

4.3. Seasonal Dependence

[37] Figure 5 summarizes the day-of-year and local time dependence of the empirical models (except for that of Thule, for which there is insufficient coverage to establish the seasonal dependence). Note the different day-of-year axes for the northern and southern hemisphere stations; in each case the seasonal axis is centered on the winter solstice, and the meridional winds are shown as positive-poleward. The South Pole meridional and zonal wind components were inferred from the 60°W and 105°W meridional wind models, as described in section 3.3. For the moderate solar EUV conditions represented in this figure, the winds over Arequipa, Arecibo, Millstone Hill, and Søndre Strømfjord show a predominately annual variation, although at Arequipa and Søndre Strømfjord a semi-annual component cannot be ruled out, due to the lack of coverage during the summer months. The seasonal patterns over Arequipa and Arecibo (which are at conjugate geographic latitudes) are quite similar, with the former showing stronger wind magnitudes.

[38] Within the limited seasonal coverage afforded by the Halley and South Pole data sets, the day-of-year dependence depicted in Figure 5 is generally weak (over an entire year, however, a strong seasonal dependence is certainly expected, given the change from nighttime to continuously sunlit conditions). In the eastern longitude sectors, however, the South Pole meridional winds do exhibit a strong day-of-year dependence within the winter season, as shown in Figure 6. In this case, the meridional winds increase in magnitude toward the equinoxes. The South Pole intra-seasonal effects are strongest in these longitude sectors and between 0800 and 1600 LT.

[39] Although the seasonal variations are generally symmetric around the winter solstice, significant differences

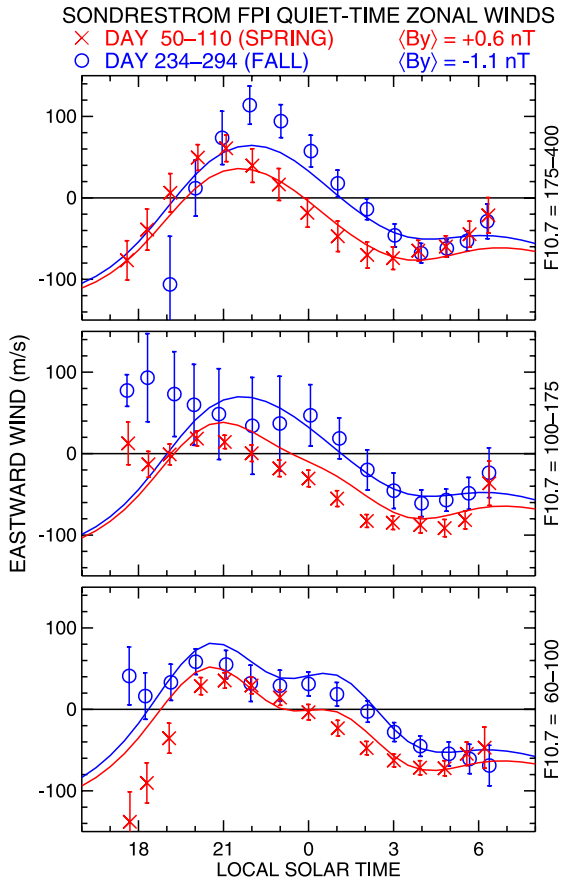

Figure 7. Average quiet time Søndre Strømfjord zonal winds as a function of local time (2-hour overlapping bins spaced at 1-hour intervals), for three solar EUV irradiance conditions: (bottom) low, (middle) moderate, and (top) high. Results are shown for two 60-day bins centered on the September (day-of-year 234–294, blue circles) and March (day-of-year 50–110, red crosses) equinoxes. Error bars denote the estimated uncertainty of the mean. The smooth curves show corresponding results from the empirical model.

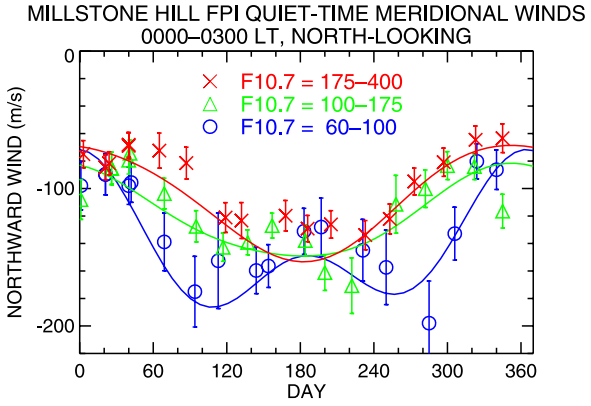

Figure 8. Average quiet time Millstone Hill north-looking meridional winds as a function of day-of-year (46-day overlapping bins spaced at 23-day intervals), in the 0000–0300 LT sector. Results are shown for three solar EUV irradiance conditions: low (blue circles, $F_{10.7} \leq 100$), moderate (green triangles, $100 \leq F_{10.7} \leq 175$), and high (red crosses, $F_{10.7} \geq 175$). Error bars denote the estimated uncertainty of the mean. The smooth curves show corresponding results from the empirical model.

between the two equinoxes can be detected in the Søndre Strømfjord zonal winds. Figure 7 shows the average zonal winds as a function of local time, with results from the March and September equinoxes superimposed. Between about 2100 LT and 0300 LT, the September winds are up to 80 m/s more eastward than the March winds. This effect appears to be partly due to a seasonal effect in the distribution of IMF B_y. Under quiet conditions, the average B_y for the data set is −1.1 nT in September and +0.6 nT in March. The midnight zonal winds at Søndre Strømfjord are more eastward under negative B_y conditions, as discussed in more detail in Paper 2, with a typical slope of −12 m/s per nT. The sampling of B_y could therefore give rise to equinoctial differences of at least 20 m/s, and possibly more, since the empirical model may have absorbed some of the IMF dependence into the seasonal variation.

[40] An equinoctial asymmetry has also been observed in high-latitude winds over Kiruna, Sweden (68°N, 20°E), but in the meridional component, and with quiet and disturbed conditions combined [*Aruliah et al.*, 1991]. The equatorward winds in the midnight sector are stronger during March than September, and this asymmetry has been attributed to UT-dependent equinoctial differences in average solar wind-magnetosphere coupling [*Aruliah et al.*, 1996]: The UT variation of the average coupling has a maximum at 2200 UT (near midnight at Kiruna) during March, and a minimum at 2200 UT during September. This effect should not influence winds at the longitude of Søndre Strømfjord [*Aruliah et al.*, 1996], since the average coupling at 0300 UT (near midnight at Søndre Strømfjord) is about the same for March and September. We therefore conclude that the equinoctial asymmetries observed at Søndre Strømfjord and Kiruna are at best indirectly related.

4.4. Coupled Seasonal/EUV Dependence

[41] For the most part, the seasonal variation is largely independent of the level of solar activity (see Figure 6, for example). However, there are two cases in which the day-of-year and $F_{10.7}$ dependences are noticeably coupled. *Emmert et al.* [2003] found that the meridional winds to the north of Millstone Hill show a strong semiannual variation only during solar minimum, when the strongest equatorward winds occur during the equinoxes. This feature is depicted in Figure 8, which shows the average meridional winds in the 0000–0300 LT sector as a function of day-of-year, with results from three $F_{10.7}$ bins superimposed, along with corresponding results from our empirical model. A semi-annual variation is also apparent in the Arecibo zonal winds around midnight, as shown in Figure 9. In this case, however, the semiannual component only occurs at solar maximum.

[42] Arecibo and Millstone Hill are the only two data sets with complete seasonal coverage; the fact that the other data sets do not exhibit a strong season-solar cycle coupling may be partly because they are limited to winter and equinox conditions. For the high-latitude winds, it seems likely that such a coupling exists, since one would expect a different response to solar EUV changes on the dayside (summer) than on the nightside (winter).

5. Conclusion

[43] Using extensive ground-based FPI measurements, we have analyzed the quiet time climatology of nighttime upper thermospheric winds over seven stations at a wide variety of latitudes. We have developed empirical representations of the quiet time winds as a function of local solar time, $F_{10.7}$, day of year, and IMF B_y; the model parameterization and coefficients are provided in the auxiliary material, and computer code for evaluating the models is available at http://cedarweb.hao.ucar.edu/tools/empirical_models.html. Our results extend and unify previous climatological analyses of measurements from these stations.

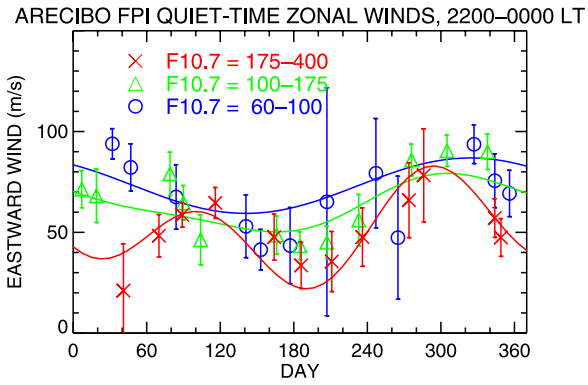

Figure 9. Average quiet time Arecibo zonal winds as a function of day of year (60-day overlapping bins spaced at 30-day intervals), in the 2200–0000 LT sector. Results are shown for three solar EUV irradiance conditions: (blue circles, $F_{10.7} \leq 100$), moderate (green triangles, $100 \leq F_{10.7} \leq 175$), and high (red crosses, $F_{10.7} \geq 175$). Error bars denote the estimated uncertainty of the mean. The smooth curves show corresponding results from the empirical model.

[44] At most latitudes and local times, the $F_{10.7}$ dependence of the winds either weakens or saturates around $F_{10.7}$ = 150, and a piecewise linear fit is therefore required to accurately represent this dependence. At two middle- and low-latitude stations, wind magnitudes decrease with increasing $F_{10.7}$, but at high latitudes and at the magnetic equator, $F_{10.7}$ has a consistently positive effect on wind speeds. These results may reflect the latitude-dependent balance between solar-driven pressure gradients and ion drag (which is a momentum source at high latitudes), both of which increase with increasing solar EUV irradiance, but the solar cycle dependence of the height of the measured emission makes interpretation difficult.

[45] For stations whose seasonal coverage is at least 8 months out of the year, the winds generally exhibit an annual variation, with extrema at the solstices (or at least the winter solstice). We found two instances, however, in which the winds exhibit a semiannual variation: meridional winds at upper midlatitudes during solar minimum, and zonal winds at low latitudes during solar maximum. Within the limited seasonal coverage (less than 6 months) afforded by two high-latitude southern stations, the day-of-year dependence is generally weak. However, winds measured from the Southern geographic pole along the meridian directed toward the south magnetic pole show a strong intraseasonal dependence, with wind speeds that increase toward equinox.

[46] In this paper we have focused on the local time, solar cycle, and seasonal variation of the quiet time winds. In our companion paper we analyze the high-latitude circulation in more detail, including the effects of IMF B_y.

[47] **Acknowledgments.** We thank S. Vennerstrom at the Danish National Space Center for providing the IMF proxy values. J. T. Emmert was supported by the National Science Foundation (Aeronomy Program, award ATM-0407823). The FPI wind data were obtained from the NSF-supported CEDAR database at the National Center for Atmospheric Research. The investigations associated with the University of Washington were supported in part by grants OPP-0229251 and ATM-010935 from NSF. The Arequipa FPI observatory was supported by NSF with grants to Clemson University and University of Pittsburgh. The Arecibo Observatory is operated by Cornell University under a cooperative agreement with NSF.

[48] Zuyin Pu thanks Roger W. Smith and Barbara Emery for their assistance in evaluating this paper.

References

Aruliah, A. L., D. Rees, and A. Steen (1991), Seasonal and solar cycle variations in high-latitude thermospheric winds, *Geophys. Res. Lett.*, *18*, 1983–1986.

Aruliah, A. L., A. D. Farmer, D. Rees, and U. Brandstrom (1996), The seasonal behavior of high-latitude thermospheric winds and ion velocities observed over one solar cycle, *J. Geophys. Res.*, *101*, 15,701–15,711.

Biondi, M. A., and D. P. Sipler (1985), Horizontal and vertical winds and temperatures in the equatorial thermosphere: Measurements from Natal, Brazil during August–September 1982, *Planet. Space. Sci.*, *33*, 817–823.

Biondi, M. A., J. W. Meriwether, and B. G. Fejer (1990), Seasonal variations in the equatorial thermospheric wind measured at Arequipa, Peru, *J. Geophys. Res.*, *95*, 12,243–12,250.

Biondi, M. A., J. W. Meriwether, B. G. Fejer, S. A. Gonzales, and D. C. Hallenbeck (1991), Equatorial thermospheric wind changes during the solar cycle: Measurements at Arequipa, Peru, *J. Geophys. Res.*, *96*, 15,917–15,930.

Biondi, M. A., S. Y. Sazykin, B. G. Fejer, J. W. Meriwether, and C. G. Fesen (1999), Equatorial and low-latitude thermospheric winds: Measured quiet time variations with season and solar flux from 1980 to 1990, *J. Geophys. Res.*, *104*, 17,091–17,106.

Buonsanto, M. J., and O. G. Witasse (1999), An updated climatology of thermospheric winds and *F* region ion drifts over Millstone Hill, *J. Geophys. Res.*, *104*, 24,675–24,687.

Buonsanto, M. J., J. C. Foster, and D. P. Sipler (1992), Observations from Millstone Hill during the geomagnetic disturbance of March and April 1990, *J. Geophys. Res.*, *97*, 1225–12,343.

Burnside, R. G., and C. A. Tepley (1989), Optical observations of thermospheric neutral winds at Arecibo between 1980 and 1987, *J. Geophys. Res.*, *94*, 2711–2716.

Burnside, R. G., F. A. Herrero, J. W. Meriwether Jr., and J. C. G. Walker (1981), Optical observations of thermospheric dynamics at Arecibo, *J. Geophys. Res.*, *86*, 5532–5540.

Crickmore, R. I. (1994), Mean thermospheric winds observed from Halley, Antarctica, *Ann. Geophys.*, *12*, 1101–1113.

DeBoor, C. A. (1978), *A Practical Guide to Splines. Appl. Math. Sci.*, vol. 23, Springer, New York.

Dickinson, R. E., E. C. Ridley, and R. G. Roble (1984), Thermospheric general circulation with coupled dynamics and composition, *J. Atmos. Sci.*, *41*, 205–219.

Duboin, M.-L., and M. Lafeuille (1992), Thermopheric dynamics above Saint-Santin: Statistical study of the data set, *J. Geophys. Res.*, *97*, 8671–8861.

Emmert, J. T., B. G. Fejer, C. G. Fesen, G. G. Shepherd, and B. H. Solheim (2002), Altitude dependence of mid and low latitude daytime thermospheric disturbance winds measured by WINDII, *J. Geophys. Res.*, *107*(A12), 1483, doi:10.1029/2002JA009646.

Emmert, J. T., B. G. Fejer, and D. P. Sipler (2003), Climatology and latitudinal gradients of quiet time thermospheric neutral winds over Millstone Hill from Fabry-Perot interferometer measurements, *J. Geophys. Res.*, *108*(AX), 1196, doi:10.1029/2002JA009765.

Emmert, J. T., G. Hernandez, M. J. Jarvis, R. J. Niciejewski, D. P. Sipler, and S. Vennerstrom (2006), Climatologies of nighttime upper thermospheric winds measured by ground-based Fabry-Perot Interferometers during geomagnetically quiet conditions: 2. High-latitude circulation and IMF dependence, *J. Geophys. Res.*, *111*, A12303, doi:10.1029/2006JA011949.

Faivre, M., J. W. Meriwether, C. G. Fesen, and M. A. Biondi (2006), Climatology of the midnight temperature maximum phenomenon at Arequipa, Peru, *J. Geophys. Res.*, *111*, A06302, doi:10.1029/2005JA011321.

Fejer, B. G., E. R. de Paula, S. A. Gonzalez, and R. F. Woodman (1991), Average vertical and zonal F region plasma drifts over Jicamarca, *J. Geophys. Res.*, *96*, 13,901–13,906.

Fejer, B. G., J. T. Emmert, and D. P. Sipler (2002), Climatology and storm-time dependence of nighttime thermospheric neutral winds over Millstone Hill, *J. Geophys. Res.*, *107*(A5), 1052, doi:10.1029/2001JA000300.

Fesen, C. G., R. E. Dickinson, and R. G. Roble (1986), Simulation of thermospheric tides at equinox with the NCAR thermospheric general circulation model, *J. Geophys. Res.*, *91*, 4471–4489.

Griffin, E. M., A. Aruliah, I. C. F. Muller-Wodarg, and A. Aylward (2004), Comparison of high-latitude thermospheric meridional winds II: Combined FPI, radar, and model climatologies, *Ann. Geophys.*, *22*, 863–876.

Hagan, M. E. (1993), Quiet time upper thermospheric winds over Millstone Hill between 1984 and 1990, *J. Geophys. Res.*, *98*, 3731–3739.

Hedin, A. E., et al. (1991), Revised global model of upper thermosphere winds using satellite and ground-based observations, *J. Geophys. Res.*, *96*, 7657–7688.

Hernandez, G., and O. A. Mills (1973), Feedback stabilized Fabry-Perot interferometer, *Appl. Opt.*, *12*, 126–130.

Hernandez, G., and R. G. Roble (1984), The geomagnetic quiet nighttime thermospheric wind pattern over Fritz Peak Observatory during solar cycle minimum and maximum, *J. Geophys. Res.*, *89*, 327–337.

Hernandez, G., R. G. Roble, and J. H. Allen (1980), Midlatitude thermospheric winds and temperatures and their reaction to the auroral electrojet activity indices, *Geophys. Res. Lett.*, *7*, 677–680.

Hernandez, G., R. W. Smith, R. G. Roble, J. Gress, and K. C. Clark (1990), Thermospheric dynamics at the south pole, *Geophys. Res. Lett.*, *17*, 1255–1258.

Hernandez, G., F. G. McCormac, and R. W. Smith (1991), Austral thermospheric wind circulation and interplanetary magnetic field orientation, *J. Geophys. Res.*, *96*, 5777–5783.

Igi, S., W. L. Oliver, and T. Ogawa (1999), Solar cycle variations of the thermospheric meridional wind over Japan derived from measurements of h_mF_2, *J. Geophys. Res.*, *104*, 22,427–22,431.

Kawamura, S., Y. Otsuka, S.-R. Zhang, S. Fukao, and W. L. Oliver (2000), A climatology of middle and upper atmosphere radar observations of thermospheric winds, *J. Geophys. Res.*, *105*, 12,777–12,788.

Killeen, T. L., B. C. Kennedy, P. B. Hays, and D. H. Ceckowski (1983), An image plane detector for the Dynamics Explorer Fabry-Perot interferometer, *Appl. Opt.*, *22*, 3503–3513.

Killeen, T. L., Y.-I. Won, R. J. Niciejewski, and A. G. Burns (1995), Upper thermosphere winds and temperatures in the geomagnetic polar cap: Solar

cycle, geomagnetic activity, and interplanetary magnetic field dependencies, *J. Geophys. Res.*, *100*, 21,327–21,342.
Link, R., and L. L. Cogger (1988), A reexamination of the O I 6300-Å nightglow, *J. Geophys. Res.*, *93*, 9883–9892.
McCormac, F. G., and R. W. Smith (1984), The influence of the interplanetary magnetic field Y component on ion and neutral motions in the polar thermosphere, *Geophys. Res. Lett.*, *11*, 935–938.
Meriwether, J. W., Jr., and P. Shih (1987), On the nighttime signatures of thermospheric winds observed at Sondrestrom, Greenland, as correlated with interplanetary magnetic field parameters, *Ann. Geophys.*, *5A*, 329–336.
Meriwether, J. W., J. P. Heppner, J. D. Stolarik, and E. M. Wescott (1973), Neutral winds above 200 km at high latitudes, *J. Geophys. Res.*, *78*, 6643–6661.
Meriwether, J. M., Jr., C. A. Tepley, S. A. Prince, and P. B. Hays (1983), Remote ground-based observations of terrestrial airglow emissions and thermospheric dynamics at Calgary, Alberta, Canada, *Opt. Eng.*, *22*, 128–131.
Meriwether, J. W., Jr., T. L. Killeen, F. G. McCormac, A. G. Burns, and R. G. Roble (1988), Thermospheric winds in the geomagnetic polar cap for solar minimum conditions, *J. Geophys. Res.*, *93*, 7478–7492.
Meriwether, J. W., M. A. Biondi, F. A. Herrero, C. G. Fesen, and D. C. Hallenback (1997), Optical interferometric studies of the nighttime equatorial thermosphere: Enhanced temperatures and zonal wind gradients, *J. Geophys. Res.*, *102*, 20,041–20,058.
Miller, K. L., M. Lemon, and P. G. Richards (1997), A meridional wind climatology from a fast model for the derivation of meridional winds from the height of the ionospheric *F2* region, *J. Atmos. Terr. Phys.*, *59*, 1805–1822.
Niciejewski, R. J., et al. (1989), Coordinated satellite and ground-based measurements of the energy characteristics of a sun-aligned arc over Søndre Strømfjord, *J. Geophys. Res.*, *94*, 17,201–17,213.
Richmond, A. D. (1995), Ionospheric electrodynamics using Magnetic Apex Coordinates, *J Geomagn. Geoelectr.*, *47*, 191–212.
Richmond, A. D., C. Lathuillere, and S. Vennerstroem (2003), Winds in the high-latitude lower thermosphere: Dependence on the interplanetary magnetic field, *J. Geophys. Res.*, *108*(A2), 1066, doi:10.1029/2002JA009493.
Rishbeth, H. (1977), Drifts and winds in the polar F regions, *J. Atmos. Terr. Phys.*, *39*, 111–116.
Roble, R. G., R. E. Dickinson, and E. C. Ridley (1982), Global circulation and temperature structure of themosphere with high-latitude plasma convection, *J. Geophys. Res.*, *87*, 1599–1614.
Sipler, D. P., M. E. Hagan, M. E. Zipf, and M. A. Biondi (1991), Combined optical and radar wind measurements in the F Region over Millstone Hill, *J. Geophys. Res.*, *96*, 21,255–21,262.
Stewart, R. D. (1986), Observations of thermospheric winds by an optical Doppler method in Antarctica, Ph.D. thesis, Univ. of Ulster, Ireland.
Stewart, R. D., R. W. Smith, D. Rees, J. R. Dudeney, and A. S. Rodger (1985), First measurements of thermospheric winds in Antarctica by an optical ground-based method, *Nature*, *317*, 45–47.
Vennerstroem, S., B. Zieger, and E. Friis-Christensen (2001), An improved method of inferring interplanetary sector structure, *J. Geophys. Res.*, *106*, 16,011–16,020.
Wickwar, V. B., J. W. Meriwether, P. B. Hays, and A. F. Nagy (1984), The meridional thermospheric neutral wind measured by radar and optical techniques in the auroral region, *J. Geophys. Res.*, *89*, 10,987–10,998.

J. T. Emmert, E. O. Hulburt Center for Space Research, U. S. Naval Research Laboratory, Code 7643, 4555 Overlook Avenue, SW, Washington, DC 20375, USA. (john.emmert@nrl.navy.mil)

M. L. Faivre and J. W. Meriwether, Department of Physics and Astronomy, Clemson University, 312 Kinard Laboratory, Clemson, SC 29631, USA.

G. Hernandez, Department of Earth and Space Sciences, University of Washington, Box 351310 Seattle, WA 98195-1310, USA.

M. J. Jarvis, British Antarctic Survey, High Cross, Madingley Road, Cambridge CB3 0ET, UK.

R. J. Niciejewski, Space Physics Research Laboratory, University of Michigan, Ann Arbor, MI 48109, USA.

D. P. Sipler, Haystack Observatory, Massachusetts Institute of Technology, Westford, MA 01886, USA.

C. A. Tepley, Arecibo Observatory, HC-03 Box 53995, Arecibo, Puerto Rico 00612.